MINISTRY OF EDUCATION
AND TRAINING

VIETNAM ACADEMY OF SCIENCE
AND TECHNOLOGY

GRADUATE UNIVERSITY OF SCIENCE AND TECHNOLOGY

Phung Thi Lan Huong

MoS_2 AND Cu_2MoS_4 NANOMATERIALS – BASED ELECTROCHEMICAL SENSOR FOR PHARAMACEUTICAL ANALYSIS

SUMMARY OF DISSERTATION ON INORGANIC CHEMSISTRY
Code: 9 44 01 13

The dissertation is completed at: Graduate University of Science and Technology, Vietnam Academy Science and Technology

Supervisors:

1. Supervisor 1: PhD. Vu Ngoc Phan
2. Supervisor 2: PhD. Nguyen Duc Anh

Referee 1: Assoc. Prof., PhD. Pham Duc Thang

Referee 2: Assoc. Prof., PhD. Lê Hải Đăng

Referee 3: Assoc. Prof., PhD. Lê Trọng Lư

The dissertation will be examined by Examination Board of Graduate University of Science and Technology, Vietnam Academy of Science and Technology at 9am on May 29, 2024.

The dissertation can be found at:

1. Graduate University of Science and Technology Library
2. National Library of Vietnam

LIST OF THE PUBLICATIONS RELATED TO THE DISSERTATION

1. **Thi Lan Huong Phung**, Ngoc Phan Vu, Tuan Anh Nguyen, Ngoc Huyen Nguyen, Xuan Dinh Ngo, Van Hoi Bui, Ly T. Le, Anh D. Nguyen, Anh-Tuan Le, Copper Molybden (IV) sulfide (Cu_2MoS_4) nanoplates as a proficient electrocatalytic interface for enhancing the electrochemical redox signals of ofloxacin for detection in pharmaceutical samples, New J. Chem., 2023, 47, 3714, doi.org/10.1039/D2NJ06098A.

2. Thai D. Nguyen, **Huong T. L. Phung**, Duc N. Nguyen, Anh D. Nguyen, Phong D. Tran, Fabrication of inverse opal molybdenum sulfide and its use as a catalyst for H2 evolution, RSC Adv., 2023, 13, 27923, DOI: 10.1039/d3ra02972g.

3. **Phùng Thị Lan Hương**, Nguyễn Đức Anh, Ngô Xuân Đinh, Nguyễn Tuấn Anh, Nguyễn Ngọc Huyền, Vũ Ngọc Phan, "Nghiên cứu chế tạo và khảo sát tính chất MoS_2 định hướng ứng dụng trong cảm biến điện hóa phát hiện Paracetamol trong dược phẩm". Hội nghị Vật lý Chất rắn và Khoa học Vật liệu Toàn quốc – SPMS 2023.

4. **Phùng Thị Lan Hương**, Vũ Ngọc Phan, Ngô Xuân Đinh, Nguyễn Đức Anh, Nguyễn Huyền Trang, Chu Xuân Quang, Hoàng Văn Tuấn, Nghiên cứu chế tạo cảm biến nano điện hóa trên cơ sở tấm nano Cu_2MoS_4 nhằm phân tích hàm lượng Chloramphenicol trong mẫu dược phẩm, Tạp chí phân tích Lý Hóa và Sinh học, Số 2 năm 2023.

5. **Thi Lan Huong Phung**, Tuan Anh Nguyen, Xuan Dinh Ngo, Ngoc Phan Vu, Anh D. Nguyen, Anh-Tuan Le, Copper molybdenum sulfide nanocatalysts-based electrochemical sensor for electro-oxidation of ofloxacin: delineating the combined roles of crystallinity and morphology on the electrocatalytic activity and analytical performance, Chemistry - An Asian Journal, 2024, doi.org/10.1002/asia.202400166.

INTRODUCTION

1. Rationale

The development of electrochemical sensors for the purpose of quantification in pharmaceutical and clinical samples faces difficulties such as low concentrations of substances in analytical samples, high accuracy for each measurement.

MoS_2 has outstanding properties such as large specific surface area, high biocompatibility, and good electron transport ability. The biggest disadvantage of MoS_2 is its poor electrical conductivity and easy clumping during the process of coating the electrode, which reduces the sensitivity and durability of the sensor. Copper molybdenum sulfide (Cu_2MoS_4) material has been manufactured and proved to be highly effective in enhancing electrical conductivity and improving electrocatalytic efficiency, minimizing clumping, thereby enhancing electrochemical performance, and increasing the durability of the sensor.

Based on the scientific basis and practical requirements, the PhD candidate has chosen the project:: ***"MoS_2 and Cu_2MoS_4 nanomaterials-based electrochemical sensor for pharmaceutical analysis"*** for a doctoral thesis.

2. Objectives of the thesis

- Survey and evaluate the chemical and physical properties of MoS_2 material and Cu_2Mo_4 material.

- Research the influence of morphology, nanostructure and material properties of MoS_2 and Cu_2Mo_4 on the electrochemical activity of the sensor during the analysis of CAP, PAR and OFX.

- Analyze CAP, PAR and OFX in pharmaceutical samples using electrochemical sensors based on MoS_2 material and Cu_2Mo_4 material.

3. Content of the thesis

Content 1: Synthesize MoS_2 nanomaterials using solvothermal and electrochemical deposition methods.

Content 2: Synthesize Cu_2Mo_4 material by hydrothermal method.

Content 3: Research to determine the chemical and physical properties of MoS_2 material and Cu_2Mo_4 material. Research the factors affecting electrochemical performance.

Content 4: Develop an electrochemical sensor to determine CAP, PAR and OFX concentrations basing on MoS_2 and Cu_2MoS_4 nanomaterials. Research the factors affecting electrochemical performance.

Content 5: Develop an analytical process to detect CAP, PAR and OFX concentrations in pharmaceutical samples.

4. Scientific and practical basis of the topic;

The thesis is conducted on the basis of experimental research results and a system of published research works. Specifically, MoS_2 material is synthesized by solvent heating method, electrochemical deposition method, Cu_2Mo_4 material is synthesized by hydrothermal method.

5. Novel contributions of the thesis

- The thesis is the first scientific work to research, evaluate and clarify the relationship between the structure - properties - electrochemical activity of the materials MoS_2 and Cu_2MoS_4 in the electrochemical detection process. CAP, PAR and OFX.

- The thesis has proven that the presence of Cu in Cu_2MoS_4 material helps enhance electrical conductivity and electrocatalytic ability, thereby increasing the sensitivity of the sensor compared to MoS_2 material.

- For the first time, the Cu_2MoS_4 material system is applied in manufacturing electrochemical sensors to determine CAP, PAR and OFX in pharmaceutical samples.

- The thesis has developed a process for analyzing CAP, PAR and OFX in pharmaceutical samples using electrochemical methods. This process can be applied in monitoring and testing pharmaceutical quality in practice.

Chapter 1 OVERVIEW

Chapter 1 introduces the status of research and development to improve the electrochemical detection efficiency of Ofloxacin (OFX), Chloramphenicol (CAP) and Paracetamol (PAR). Among the methods of improving electrochemical efficiency, the method of using nanomaterials and modifying the working electrode is easy to implement and highly effective.

Chapter 1 also presents potential materials used for developing electrochemical sensor systems. On that ground, the scientific basis for choosing suitable materials for research in the next chapters such as MoS_2, Cu_2MoS_4 is outlined. From an overview of the research situation and published results, it can be seen that research on electrochemical sensors to detect OFX, PAR and CAP from materials MoS_2, Cu_2MoS_4 has not received much attention. Research only focuses on studying the application of MoS_2, Cu_2MoS_4 in energy storage and conversion. Therefore, investigating the fabrication and effects of the morphology of MoS_2, Cu_2MoS_4 materials on the electrochemical performance of OFX, CAP and PAR detection will contribute to improving the properties and detection ability of electrochemical sensors based on the above two materials, diversifying their applications.

Chapter 2 EXPERIMENT

In this chapter, two material systems MoS_2 and Cu_2MoS_4 (CMS) are synthesized by solvothermal and hydrothermal methods. Material characterization methods include: scanning electron microscope (SEM); energy dispersive X-ray spectroscopy (EDX); X-ray diffraction (XRD) method; Raman spectroscopy and electrochemical methods such as cyclic potential scanning (CV), differential pulse potential scanning (DPV), impedance spectroscopy (EIS), are described in terms of operating principle, meaning and applications.

2.1. MATERIALS AND CHEMICALS

2.1.1. MATERIALS FABRICATION

2.1.2. Synthesis of MoS_2 nanoplates

2.1.3. Synthesis of Cu_2MoS_4 nanoplates

2.1.4. Preparation of the modified electrode

2.2. METHODS

2.2.1. Instrumental characterization

2.2.2. Electrochemical methods

2.2.3. Analytical procedures

Chapter 3 RESULTS AND DISCUSSION

3.1. MOLYBDENDEN SUNFIDE MATERIAL SYSTEM

3.1.1. Microstructures and Characterization of NP- MoS_2 material

As illustrated in Figure 3.1 (a-d), the morphology of NP-MoS_2, synthesized via the solvothermal method, adopts a configuration akin to spherical-like nanoparticles, with an average size of 46,21 nm and the atomic ratio of Mo/S is about 1/2. This distinctive structure of the synthesized NP-MoS_2 holds the promise of a larger surface area, implying a greater active site availability for the adsorption of OFX, CAP and PAR.

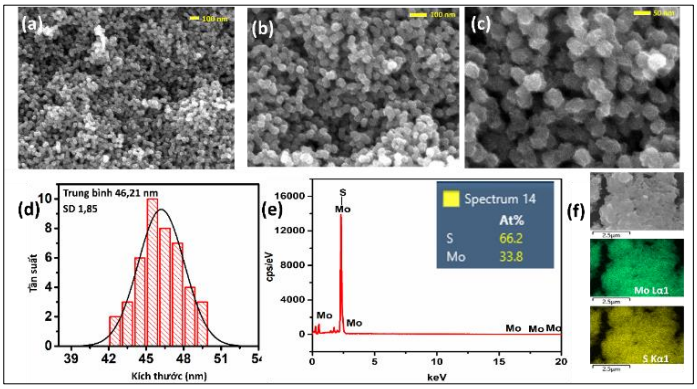

Figure 3.1. SEM images (a, b, c), size distribution chart (d), EDX diagram and EDX mapping image of NP-MoS_2 material (e, f).

The crystal microstructure of the as-synthesized NP-MoS_2 was determined by X-ray diffraction in Figure 3.2 a. The diffraction peaks were observed at 2θ = 13,23°; 33,4°; 59,12° representing the (002); (101) and (110) crystal planes of MoS_2 molybdenite-2H. The obtained Raman spectra reveals two characteristic vibration modes within the MoS_2 molecule in the frequency range of E_1^{2g}, A_{1g} (Figure 3.2 b). The Raman band located at 380 cm^{-1} can be assigned to the E_1^{2g} mode, the mode at 400 cm^{-1} is assigned to A_{1g} mode, corresponding to the Mo-S bond, there is also a vibration at 223 cm^{-1} corresponding to the Mo-Mo bond.

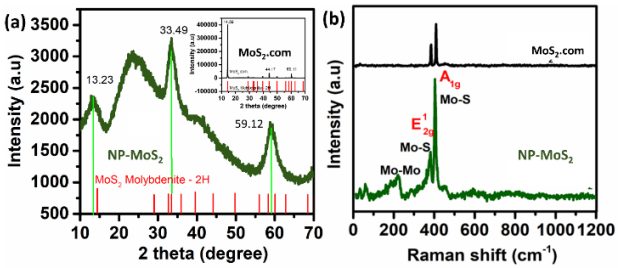

Figure 3.2. X-ray diffraction pattern (a) and raman spectrum (b) of NP-MoS_2 and commercial MoS_2.

Conclusion: Successfully synthesized NP-MoS_2 material with porous granular form and crystalline structure.

3.1.2. Electrochemical characteristics of NP-MoS_2/SPE electrode

The electrochemical properties of the NP-MoS_2/SPE electrode were evaluated by using CV and electrochemical impedance spectroscopy (EIS) experiments. Figure 3.3a shows the CV analysis results of bare SPE and NP-MoS_2/SPE in 0,1 M KCl containing 5 mM $K_3[Fe(CN)_6]$ and 5 mM $K_4[Fe(CN)_6]$. From obtained results, the peak-to-peak separation (ΔE_p) between oxidation and reduction potential at bare-SPE and NP-MoS_2/SPE was calculated to be about 90 mV and 139 mV, respectively. It is clearly that the ΔE_p value of CMS/SPE is lower than that of bare SPE, revealing

fast electron transfer kinetic of NP-MoS_2/SPE. In addition, after the surface modification of SPE with NP-MoS_2 nanoplates, the oxidation/reduction peak current responses were significantly improved. The calculated results show that cathodic and anodic peak currents for NP-MoS_2/SPE were 1,2-fold higher than that of bare SPE. It means that the NP-MoS_2 nanoplates possessed an excellent electrochemical characterization arising from the rich redox chemistry of both transition metal and chalcogenide ligands. The electrochemically active surface area (ECSA) of NP-MoS_2/SPE (0,2617 cm^2) was about 1,5 folds larger than that of bare-SPE (0,1784 cm^2) (Figure 3.3 b), revealing that NP-MoS_2 nanoplates can significantly enhance the electrochemical response due to their rich active sites.

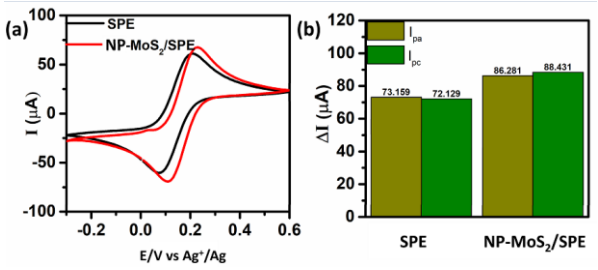

Figure 3.3. CV curve (a), bar graph comparing oxidation and reduction current intensity (b), of SPE and NP-MoS_2 /SPE in 0.1 M KCl containing 5 mM $K_3[Fe(CN)_6]$ and 5 mM $K_4[Fe(CN)_6]$.

In the Nyquist diagrams of pure-SPE and NP-MoS_2/SPE at Figure 3.4 a, the R_{ct} values of SPE and NP-MoS_2/SPE were 556,8 and 31,2 Ω, respectively. The smaller R_{ct} value of the NP-MoS_2/SPE modified electrode indicated a rapid electron transfer kinetics through the NP-MoS_2/SPE surface, because NP-MoS_2 nanoplates-modified electrode offers an enriched active surface area and excellent electron transfer ability. In addition, the electrochemical sensor based on NP-MoS_2 can operate electrochemically in the potential range from -0.4 V to 1.0 V (Figure 3.4 b).

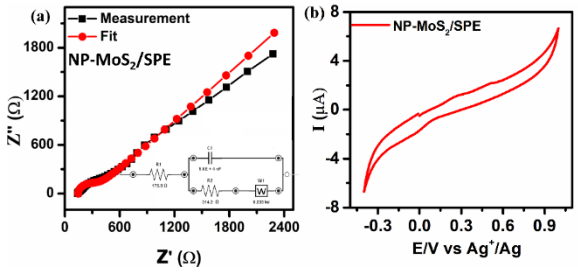

Figure 3.4. EIS spectra on SPE and NP-MoS_2/SPE in 0.1 M KCl containing 5 mM $K_3[Fe(CN)_6]$ and 5 mM $K_4[Fe(CN)_6]$ (a), CV curve of NP-MoS_2 material (b) in PBS 7,0 solution.

Conclusion: The material NP-MoS_2 is synthesized by the solvent thermal method, possessing the following characteristics: stable crystal structure; large electrochemically active surface area and capable of electrochemical activity in the range – 0,4V to + 1,0V. This material has potential applications in electrochemical sensors to determine organic compounds (OFX, PAR and CAP).

3.1.3. Electrochemical behavior of OFX, CAP and PAR of NP-MoS_2 /SPE.

3.1.3.1. Molybdenum sulfide-based sensor for determination of Ofloxacin

The electrochemical behavior of OFX on the NP-MoS_2/SPE was investigated by using LSV technique in PBS (pH = 7,0) containing 100 μM OFX at a scan rate of 10 mV s^{-1}. The improved electrocatalytic performance of the NP-MoS_2 nanoplates are further evidenced in Figure 3.5 a. Electrode NP- MoS_2/SPE capable of electrochemical enhancement of OFX (2.39 times more than SPE electrode). The reason can be explained by the porous structure and large surface area of NP-

MoS_2 particles, which increases the electrochemically active area of the working electrode, increasing the electron transfer rate. NP-MoS_2 material has the potential to be applied in electrochemical sensors to determine OFX.

Figure 3.6a shows the DPV curves of the different OFX concentrations (5,0 – 75 µM) on the NP-MoS_2 in 0,1 M PBS (pH 7,0). The peak current increased linearly with the increase of OFX concentration from 5,0 µM to 75 µM for NP-MoS_2/SPE. The obtained regression equation was: ΔI_{pc} = 0,057 C_{OFX} (µM) + 0,112, R^2 = 0,99. with the limit of detection (LOD) of 2,5 µM. The electrochemical sensitivity of the proposed electrochemical sensor reached 0,518 µA μM^{-1} cm^{-2}

3.1.3.2. Molybdenum sulfide-based sensor for determination of Chloramphenicol

Figure 3.5b shows the CV response of bare SPE and NP-MoS_2 /SPE in 0,1 M PBS (pH = 5,0) containing 100 µM CAP at different scan rates from 10 to 60 mV s^{-1}. A characterized two reduction peaks of CAP at E_{pc1} between -0,65 and -0,75 V and E_{pc2} in about -0,15 to -0,09 V appeared, corresponding to the two typical reduction processes of CAP.

Figure 3.6c shows the DPV curves of the different CAP concentrations (10 – 70 µM) on the NP-MoS_2 in 0,1 M PBS (pH 5,0). As can be seen, the peak current increased linearly with the increasing concentration of CAP from 10 µM to 70 µM for NP-MoS_2/SPE. The obtained regression equation was: ΔI_{pa} = 0,134 C_{CAP} (µM) – 0,721, R^2 = 0,98. with the limit of detection (LOD) of 5,0 µM. The electrochemical sensitivity of the proposed electrochemical sensor reached 1,22 µA μM^{-1} cm^{-2}

3.1.3.3. Molybdenum sulfide-based sensor for determination of Paracetamol

Figure 3.5c shows the CV response of bare SPE and NP-MoS_2 /SPE in 0,1 M PBS (pH = 3,0) containing 100 µM PAR at different scan rates from 10 to 60 mV s^{-1}. For the SPE electrode, the oxidation and reduction peak potentials (E_{pa} and E_{pc}) of PAR were observed at 0.370 V and − 0.070 V with the oxidation and reduction peak currents (I_{pa} and I_{pc}) calculated to be about 3.556 and 1.990 µ M, respectively, for the NP-MoS_2 /SPE electrode the I_{pa} and I_{pc} values were 1.16 and 1.34 times higher than for the bare electrode (4.131 and 2.680 µM) with E_{pa} and E_{pc} values of 0.370 and 0.040 mV, respectively.

Figure 3.6c shows the DPV curves of the different PAR concentrations (5,0 – 100 µM) on the NP-MoS_2 in 0,1 M PBS (pH 3,0). As can be seen, the peak current increased linearly with the increasing concentration of PAR from 5,0 µM to 100 µM for NP-MoS_2/SPE. The two calibration graphs obtained show a good linear relationship between the oxidation peak current and PAR concentration in the concentration range: from 5,0 to 100 µM with the regression equation as follows: ΔI_{pa} = 0,094 C_{PAR} (µM) + 1,029 (R^2 = 0,99). The limit of detection (LOD) of the electrochemical sensor was determined to be 0,76 µ M, the electrochemical sensitivity was calculated to be 0,28 µ A µ M^{-1} cm^{-2}.

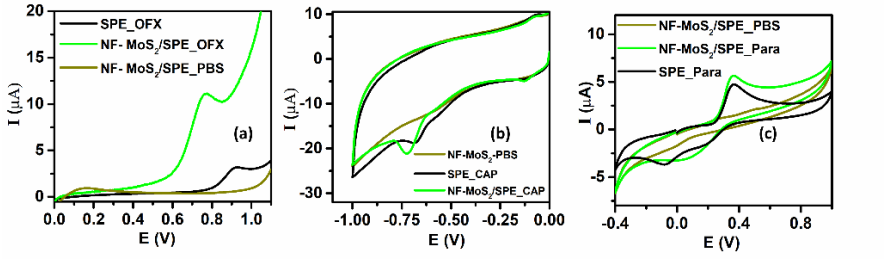

Figure 3.5. LSV and CV curves detecting OFX (a), CAP (b) and PAR (c) of NP-MoS_2/SPE and CMS30-4/SPE electrodes .

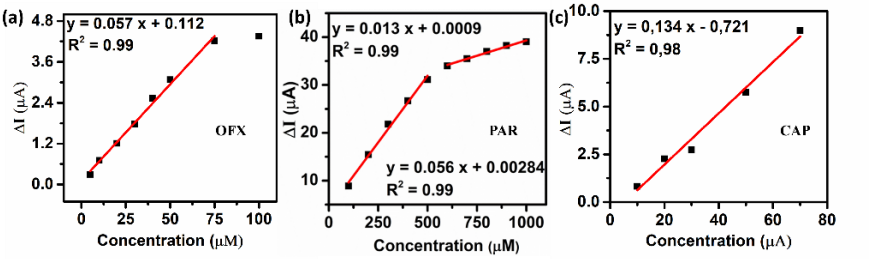

Figure 3.6. Standard curve showing the relationship between peak current intensity and OFX (a), PAR (b) and CAP (c) concentrations.

Table 3.1. Comparative study of the performance of NP-MoS_2/SPE electrode for OFX, PAR and CAP electrochemical detection .

Object	Linear range (µM)	Detection limit (µM)	Electrochemical sensitivity (µA $\mu M^{-1} cm^{-2}$)
CAP	10 - 70	5,0	1,22
OFX	5,0 - 75	2,5	0,518
PAR	100 - 500 and 500 - 1000	0,76	0,28

Conclusion: The electrochemical sensor based on NP-MoS_2 material has good performance for PAR detection electrochemical reduction, the method has high electrochemical sensitivity, relatively low detection limit and range wide linear. For CAP and OFX, sensors based on NP-MoS_2 material , it is necessary to improve the detection limit and stability.

3.2. MATERIAL SYSTEM _ COPPER MOLYBDENDEN SUNFIDE

3.2.1. Morphology and structure of CMS materials

The formation of different morphological structures of CMS NMs was studied using the FE-SEM technique, as shown in Figure 3.7. The Cu_2MoS_4/$Cu(NH_4)MoS_4$ (CMS10-3 sample) and Cu_2MoS_4 (CMS30-3 sample) nanotubes were densely packed with an approximately uniform size distribution. According to our previous report, prolonging the hydrothermal reaction time leads to the structural collapse from nanotubes to nanoplates, resulting in Cu_2MoS_4 in the form of nanoplates (CMS30-4 sample). Furthermore, the high-magnification FE-SEM image of the CMS30-4 sample indicates the CMS nanoplates are broken into many small pieces with a high density of wrinkles and interstitial spaces in-between. The EDX result confirms the formation of two phases (Cu_2MoS_4 and $Cu(NH_4)MoS_4$) in the CMS10-3 sample and the single-crystalline nature of Cu_2MoS_4 in the CMS30-3 and CMS30-4 samples.

The crystalline phase and structure of the as-synthesized CMS NMs were determined *via* X-ray diffraction, as illustrated in Figure 3.8. As can be seen, the XRD patterns of all three CMS samples have diffraction peaks at 2θ = 17,7; 18,8; 29,4; 31,4; 33,3; 35,6; 37,9; 46,4; 47,8; 49,6; 51,2; 54,6 and 57,0°, which can be indexed to (002), (011), (112), (013), (020), (004), (022), (123), (220), (024), (222), (006), and (132) crystal planes of tetragonal CMS, respectively. Nevertheless, in the XRD pattern of the CMS10-3 sample, the diffraction peaks were clearly observed at 2θ values of 15,6;

22,2; 29,9; 36,8 and 40,2°, representing the (100), (200), (211), (112) and (202) planes of $Cu(NH_4)MoS_4$ crystal, respectively (JCPDS card no. 23-0010). For the CMS30-3 and CMS30-4 samples, no additional peaks related to impurities such as $Cu(NH_4)MoS_4$, $(NH_4)_2MoS_4$, and Cu_2O were observed, indicating the single-crystalline and highly-quality of the formed Cu_2MoS_4.

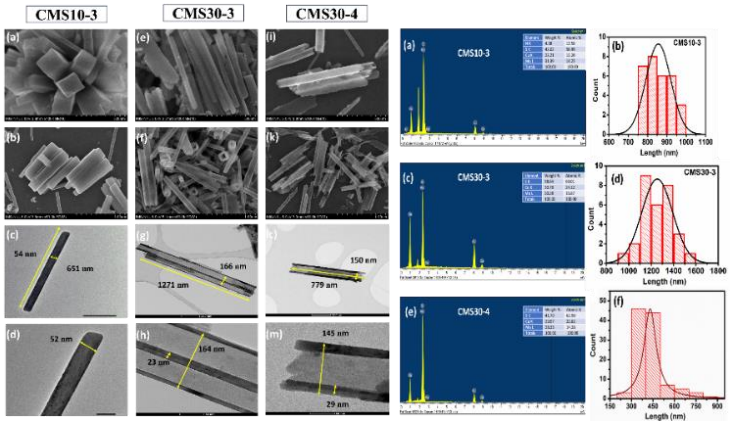

Figure 3.7. FE-SEM, TEM images with different magnifications and EDX spectrums of the CMS10-3, CMS30-3, and CMS30-4 samples. Inset the quantitative weight and atomic percentage of the compositional elements.

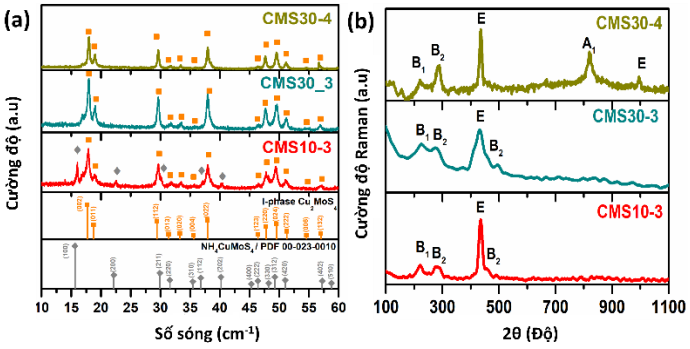

Figure 3.8. X-ray diffraction patterns (a) and Raman spectra (b) of CMS material samples.

To study the difference in the specific surface area and the adsorption capacity of the as-prepared CMS samples, the Brunauer–Emmett–Teller (BET) analysis was performed (Figure 3.9). the CMS30-4 sample achieved the highest values of the BET surface area of 204 m^2g^{-1}, which was 2,5 and 9,5 times higher than that of the CMS30-3 sample (81,2 $m^2\ g^{-1}$) and CMS10-3 sample (21,4 $m^2\ g^{-1}$), respectively. This can be attributed to the plate-like structure of CMS NMs that contain a large amount of interstitial space, which can be utilized for the efficient adsorption/desorption of ions or analytes.

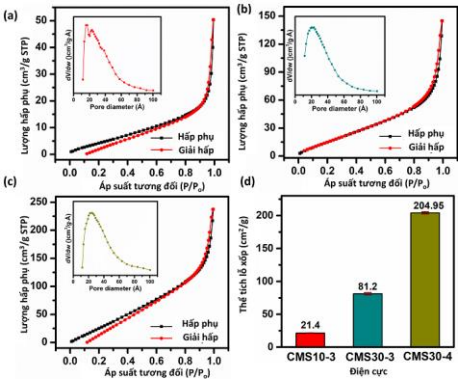

Figure 3.9. N_2 adsorption/desorption isotherms of samples (a) CMS10-3, CMS30-3 (b), CMS30-4 (c) and corresponding bar graph (d) of BET surface area.

Conclusion: The morphology and structure of CMS materials can be controlled based on controlling the reaction time and hydrothermal time. CMS material with 3 morphologies, tube-shaped structures (CMS10-3), hollow bar (CMS30-3) and nanoplates (CMS30-4) has been successfully manufactured.

3.2.2. Influence of morphology on electrochemical characteristics of electrochemical sensors based on materials CMS.

As a first step toward elucidating the roles of influence of crystallinity and morphology of CMS on the overall electrochemical kinetics, the electrochemical behavior of various un-modified and CMS-modified electrodes was studied through the CV technique using the $[Fe(CN)_6]^{3-/4-}$ redox probe Figure 3.10. Nevertheless, in comparison with the bare SPE, three CMS-modified electrodes caused a remarkable enhancement in reduction/oxidation peak currents and a decrease in the peak-to-peak potential separation (ΔE_p). As expected, the ECSA values of CMS30-3/SPE (0,223 cm^2) and CMS30-4/SPE (0,202 cm^2) were 1,64 and 1,49 times higher than that obtained on the bare SPE, 1,15 and 1,04 times higher than that obtained on the CMS10-3/SPE. The obtained results indicate obviously that the crystalline, high-quality CMS NMs with tube-/plate-shaped structures not only maintain continuous electron/ion transport channels for obtaining the maximum electron transfer rate but also supply high electroactive surface area for the efficient adsorption of analytes, which collectively improves the electrochemical sensing performance. However, the ECSA values are not replicate the difference between BET results of CMS NMs, since the ECSA strongly depends on the electron transfer process in the materials.

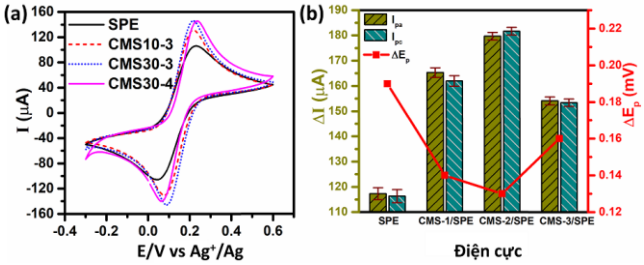

Figure 3.10. CV curve (a), bar graph comparing oxidation and reduction current intensity (b), of SPE, CMS10-3/SPE, CMS30-3/SPE, and CMS30-4/SPE electrodes in KCl solution 0.1 M contained $[Fe(CN)_6]^{3-/4-}$ 5 mM with a scan rate of 50 mV s^{-1}.

The bare SPE with the large semicircle domain in the high-frequency region with the R_{ct} value calculated at 556,8 Ω indicated high electron transfer resistance and poor electrocatalytic activity. In contrast, the R_{ct} values of CMS10-3/SPE, CMS30-3/SPE, and CMS30-4/SPE were estimated to be 302,0; 126,0; and 164,5 Ω, respectively (Figure 3.11). Modification of the working electrode by the introduction of CMS NMs with high purity and crystallinity (CMS30-3 and CMS30-4 samples) reflected the best R_{ct} results, confirming the impressive promotion in electrical conductivity and authorizing optimized electrocatalytic activity for electrochemical reactions. The calculated k^0 values of the bare SPE, CMS10-3/SPE, CMS30-3/SPE, CMS30-4/SPE are 0.70×10^{-6}, 0.91×10^{-6}, 1.89 ×

10^{-6}, and 1.33×10^{-6} cm s^{-1}, respectively. These results are consistent with the calculated results for ΔI_{pa}, ΔI_{pc}, $\Delta E_{p,}$ and ECSA values from CV measurements in $[Fe(CN)_6]^{3-/4-}$.

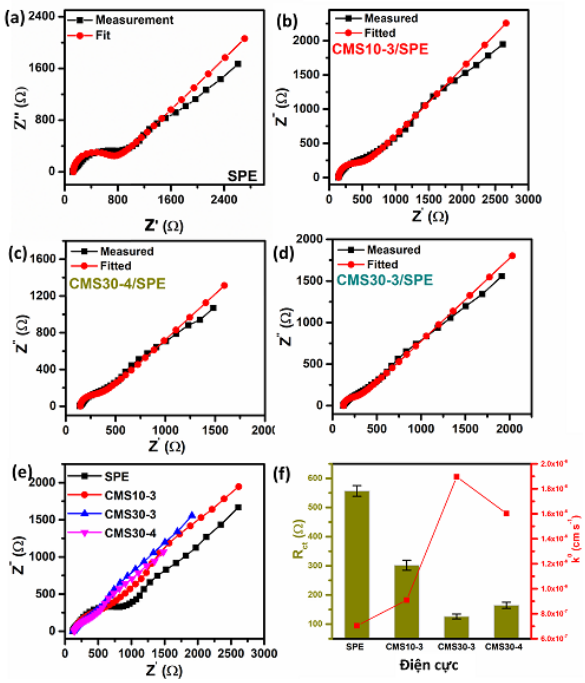

Figure 3.11. Nyquist plots measuring the impedance and Randles circuit of the SPE (a) and CMS/SPE (be) electrodes.

Conclusion: The enhancement in electrochemical activity of CMS30-3/SPE and CMS30-4/SPE can be attributed to rich catalytic active sites and more efficient multiple electron transfer pathways that arise from the synergistic coupling between the high-purity crystalline and tube- or plate-like structure of the as-synthesized Cu_2MoS_4 NMs.

3.2.3. The electrochemical kinetics of the CMS-modified SPE electrodes toward the OFX detection

As shown in Figure 3.12, by extrapolating the linear part of the LSV curves, the onset potentials (E_{onset}) for the CMS30-4/SPE showed a negative shift in the E_{onset} value of about 68, 28, and 16 mV compared to that of the bare SPE, CMS10-3/SPE, and CMS30-3/SPE, respectively, which indicates that less energy is needed for the electrochemical oxidation process of OFX at CMS30-4/SPE. In addition, the oxidation peak current of OFX recorded in CMS30-4/SPE was measured to be 23.53 µA. This value was 2.60- fold, 1.67- fold, and 1.48 -fold higher as compared to the bare SPE, CMS10-3/SPE, and CMS30-3/SPE, respectively. From the resulting oxidation peak current, the onset potential as well as the Tafel slope of the LSV study, it is evident that among the CMS NMs used in this study, the CMS30-4 sample exhibited superior electrocatalytic activity toward the electro-oxidation of OFX. The high-quality crystalline and plate-like CMS NMs (CMS30-4) accelerated the electron transfer at the electrode/electrolyte solution interface, facilitating the charge transferability to the analyte.

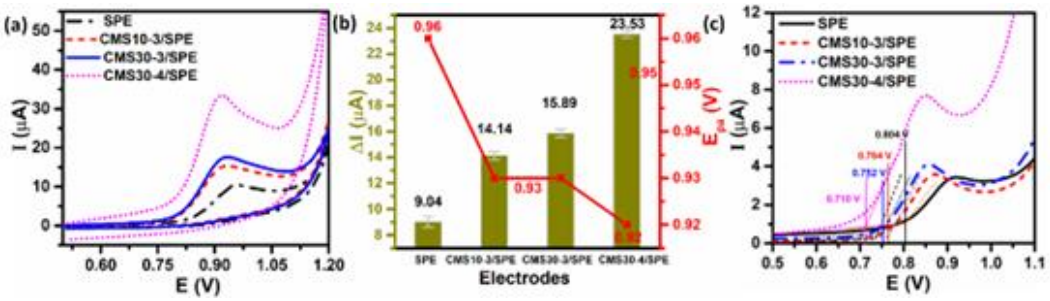

Figure 3.12. The CV curve (a) and corresponding bar graph (b), and the LSV curve (c) were recorded on SPE and CMS/SPE electrodes in 100 μM OFX solution, with a scan velocity of 10 mV/s.

Figure 3.13 presents the CV curves of 100 μM OFX in 0.1 M PBS (pH 7.0) with various scan rates from 10 to 60 mV s^{-1} and the corresponding calibration plots of oxidation peak potential *vs.* the natural logarithm of scan rate and *vs.* scan rate of the CMS10-3/SPE, CMS30-3/SPE and CMS30-4/SPE. As can be seen, the irreversible electrochemical oxidation of OFX caused the peak potential to shift in a positive direction with the increasing scan rate, with the linear relationship between the natural logarithm of the scan rate and the anodic peak potential can be expressed as:

E_{pa} (V) = 0.039 lnν (Vs^{-1}) + 1.117 (R^2 = 0.99) (CMS10-3/SPE)

E_{pa} (V) = 0.032 lnν (Vs^{-1}) + 1.036 (R^2 = 0.98) (CMS30-3/SPE)

E_{pa} (V) = 0.02 lnν (Vs^{-1}) + 0.0030 (R^2 = 0.99) (CMS30-4/SPE)

In addition, the oxidation peak current of OFX linearly increases when the scan rate increases, indicating the electrochemical oxidation of OFX toward three CMS-modified electrodes is a diffusion-controlled process. The linear regression equations were in the followings

ΔI_{pa} (μA) = 0.168 ν ($mV.s^{-1}$) + 3.214 (R^2 = 0.99) (CMS10-3/SPE)

ΔI_{pa} (μA) = 0.210 ν ($mV.s^{-1}$) + 2.537 (R^2 = 0.99) (CMS30-3/SPE)

ΔI_{pa} (μA) = 0.142 ν ($mV.s^{-1}$) + 3.186 (R^2 = 0.99) (CMS30-4/SPE)

From the intercept values from the regressions, the k_s values of CMS10-3/SPE, CMS30-3/SPE and CMS30-4/SPE was calculated to be: 0.27; 0.33 and 0.37, respectively. The larger value of k_s at the CMS30-4/SPE indicates that the high-quality crystalline and plate-like CMS accelerated the electron transfer at the electrode/electrolyte solution interface, facilitating the charge transferability to the analyte.

Adsorption capacity value (Γ) of OFX molecules on the electrodes CMS10-3/SPE, CMS30-3/SPE and CMS30-4/SPE calculated according to the above formula are: 2.41. 10^{-7}; 2.60. 10^{-7}; and 2.77. 10^{-7} $mol.cm^{-2}$ respectively. Although the A value of CMS30-3/SPE is higher than that of CMS30-4/SPE, all the electrochemical kinetic values of OFX such as ΔI_{pa} , E_{pa}, k_s and Γ,on the CMS30-4/SPE are all higher than the value of CMS30-3/SPE. This phenomenon may be related to the surface area calculated from the BET results as well as the morphology of the CMS, which was clarified in the previous section.

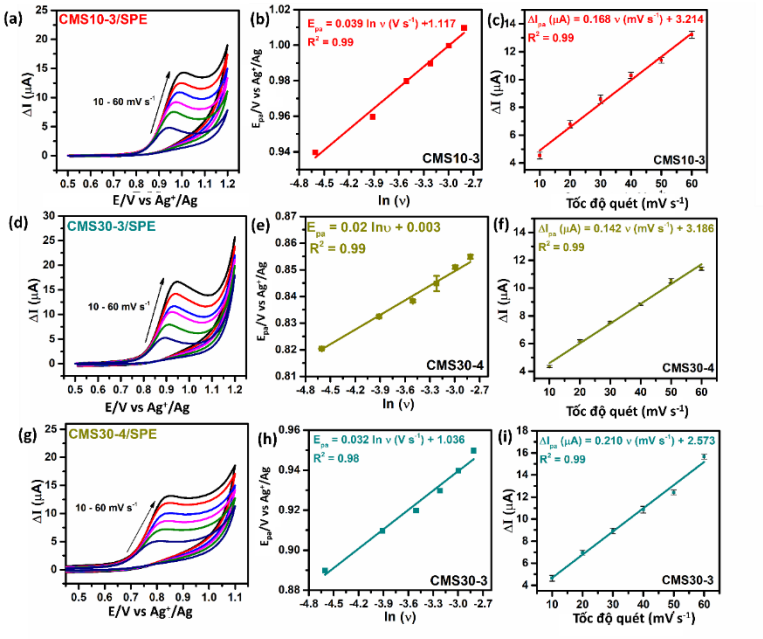

Figure 3.13. CV curves of 100 µM OFX in 0.1 M PBS (pH 7.0) with various scan rates from 10 to 60 mV s^{-1}, the corresponding calibration plots of oxidation peak potential *vs.* the natural logarithm of scan rate, and the corresponding calibration plots of oxidation peak potential *vs.* scan rate of the CMS10-3/SPE (a, b, c), CMS30-3/SPE (d, e, f), and CMS30-4/SPE (g, h, i).

Table 3.2: Comparative study of the performance of CMS modified electrodes for OFX electrochemical detection

Technique	**Unit**	**CMS10-3/SPE**	**CMS30-3/SPE**	**CMS30-4/SPE**
CV – EIS $[Fe(CN)_6]^{3-/4-}$	**A (cm^2)**	0.194	0.223	0.202
	R_{ct} (Ω)	302.0	126.0	164.5
	k^0 ($cm\ s^{-1}$)	0.91×10^{-6}	1.89×10^{-6}	1.60×10^{-6}
CV OFX 100 µM	**k_s**	0.27	0.33	0.37
	Γ	2.41×10^{-7}	2.60×10^{-7}	2.77×10^{-7}
LSV OFX 100 µM	**E_{onset} (V)**	0.764	0.752	0.710

Conclusion: The electrochemical sensor based on CMS10-3 material shows lower electrochemical activity than the other two electrodes. The reason may be due to the presence of Cu $(NH_4)MoS_4$ phase as an intermediate phase during the fabrication process, leading to reduced electrocatalytic activity of CMS10-3.

CMS30-4 is a sheet-shaped, porous structure that is expected to reveal many electrochemically active sites on the working electrode surface, helping to increase the density of electrochemical reaction sites for oxidation/reduction processes. electrochemistry on the electrode surface. CMS30-4 material has the potential to be used as a research material and to manufacture electrochemical sensors for the purpose of detecting a number of organic compounds used in medicine such as OFX,

PAR, CAP. Therefore, in the next part of the thesis, we use CMS30-4 material to fabricate an electrochemical sensor to determine OFX, CAP and PAR in pharmaceutical samples.

3.3. ELECTROCHEMICAL SENSOR BASED ON CMS30-4

3.3.1. Morphological and structural characteristics of CMS30-4 material

Figure 3.14 show representative TEM, high-angle annular dark-field (HAADF) TEM images of the CMS30-4 nanoplates, respectively. TEM images clearly reveal the plate-shaped structure of the as-obtained CMS samples with the mean length and width of 720 and 92 nm, respectively, which were very consistent with SEM results. The HAADF image further confirms the highly crystalline nature of CMS nanoplates with the crystal lattices of 0.27 and 0.53 nm with an interfacial angle of 90°, corresponding to the (020) and (002) face of Cu_2MoS_4 with a I-phase, respectively. In addition, the EDX elemental mapping results in Figure 3.14 e-h illustrate that three Cu, Mo, S elements are homogeneously distributed throughout the CMS nanoplates. The CMS nanoplates the top-tier catalysts made of CMS having different morphologies with the large specific surface area, the multi-valence of Mo together with the possibility of conversion reaction with S in as-obtained Cu_2MoS_4 nanoplates could enhance electrocatalytic activity, promising in improve the overall electrochemical sensing performance.

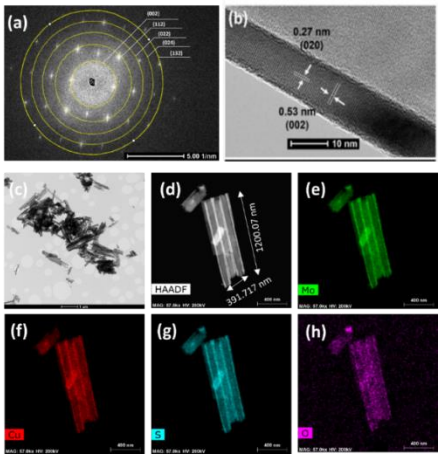

Figure 3.14. SAED image (a), HR-TEM image (b, c), EDX mapping image (dh) of sample CMS30-4.

3.3.2. Electrochemical performance of CMS30-4/SPE towards OFX

To optimize of analysis conditions, the effects of scan rate of CV and DPV techniques, pH value on the electrochemical response of the proposed electrochemical sensor for the detection of OFX were investigated. In Figure 3.15, the measurements were practiced within the conditions of 100 µM OFX at CMS30-4/SPE from pH 3.0 to pH 8.0. It can be clearly observed, at pH 4.0 the current signal has a maximum value. Thus, optimum pH 4.0 was employed for the next electrochemical measurements. Moreover, there is a linear relationship between pH and oxidation peak potential via the regression equation: $E_{pa} = -0.05\ pH + 1.11$ ($R^2 = 0.97$), owing to the oxidation peak position shift to close 0 V with the increase of pH, demonstrating that protons are involved as the product of the oxidation process of OFX. The obtained slope is -0.05 V/pH which is near the Nernst theoretical value of (- 0.059m/n) V/pH, revealing the equal number of electrons and protons. From these obtained results, the number of protons (m) which are involved in the electrochemical oxidation process of OFX were found to be 2. Therefore, the electrochemical reaction mechanism

for the OFX oxidation was the participation of two electrons and two protons, which agreed with previously reported results.

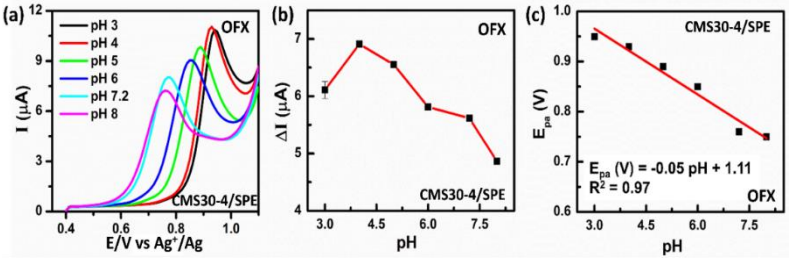

Figure 3.15. Results of investigating the influence of scanning speed (a, b, c); and pH (d, e, f) for the OFX detection ability of the CMS30-4/SPE electrode.

As shown in Figure 3.16, it is clear that the peak current increased linearly with increasing the concentration of OFX from 0.625 μM to 100 μM for CMS30-4/SPE. The obtained regression equation was I_p (μA) = 0.129 C (μM) – 0.068 (R^2 = 0.999) with the limit of detection (LOD) of 67 nM

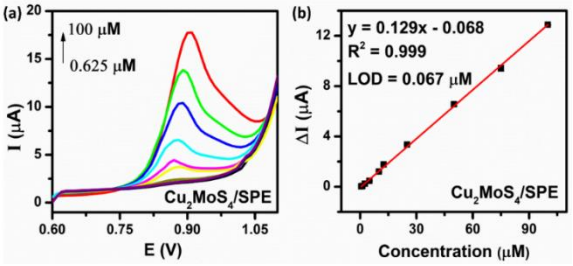

Figure 3.16: DPV curve (a) and standard curve showing the relationship between peak current intensity and OFX concentration (b) of CMS30-4/SPE in 0.1M PBS solution (pH = 4.0) containing OFX with concentrations varying from 0.625 to 100 μM.

The DPV method was used to determine the stability, selectivity and repeatability of the sensor, measurements were performed in a 0.1M PBS solution (pH = 4.0) containing OFX. Figure 3.17a shows the results of the stability survey in 3 times: day 1, day 14 and day 60 after manufacturing the CMS30-4/SPE sensor. The OFX oxidation current signal retained 98.10 % and 94.60 % of the original signal intensity after 14 and 60 days of storage at room temperature. The repeatability of the sensor is about 5.41 % for 20 repeated measurements as shown in Figure 3.17.

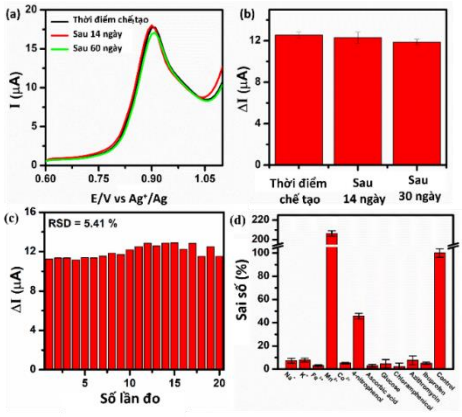

Figure 3.17: DPV curve to investigate the stability (a, b), repeatability (c), and selectivity of the CMS30-4/SPE sensor in 0.1M PBS solution (pH = 4.0) containing OFX 100 μM.

Figure 3.17d shows the results of evaluating the selectivity of electrochemical sensors by measuring the OFX oxidation current using DPV technique in the presence of common interfering compounds such as ibuprofen, glucose, azithromycin, CAP, 4-nitrophenol and metal ions Na^+, K^+, Fe^{3+}, Mn^{2+}, Co^{2+}. The results showed that a 10-fold concentration of potential interferences such as ibuprofen, glucose, CAP, and Na^+, K^+, Fe^{3+}, Co^{2+} ions had no obvious effect on detection. OFX by electrochemical method, with relative error less than 10 %. However, the presence of 4-nitrophenol and Mn^{2+} increases the relative error (29.5 - 56.5 %). Therefore, 4-nitrophenol and Mn^{2+} may affect the analytical performance for OFX detection of CMS30-4-based electrochemical sensors. All of the above-mentioned interfering compounds must be separated before performing electrochemical experiments for OFX detection.

Conclusion: The analytical parameters of the electrochemical sensor based on CMS30-4 for OFX detection were compared with several sensors reported in recent publications. These results indicate that CMS30-4 material has enhanced the electrical conductivity, and electrocatalytic activity of the SPE electrode. This material is suitable for manufacturing OFX detection sensors, for sensors with high electrochemical sensitivity, relatively low detection limit and wide linear range.

3.3.3. Electrochemical performance of CMS30-4/SPE towards CAP

To evaluate the response of the modified electrode to CAP, we used the CV scanning method, comparing the CAP redox process on two CMS30-4/SPE electrodes and the bare SPE electrode with the process redox CAP, the results are shown in Figure 3.18. In Figure 3.18 a, the CV curve of Cu_2MoS_4/SPE electrode in 0.1 M PBS buffer solution (pH = 5.0) has no electrochemical signal (no redox reaction occurs), when Adding CAP to the solution, two reduction peaks appear in the potential scanning region from -1.0 V to 0.0 V, (E_1 = -0.70 V and E_2 = -0.09 V) corresponding to two reduction processes of CAP. From this result, it shows that it is possible to analyze CAP by electrochemical method with modified electrodes based on CMS30-4 material.

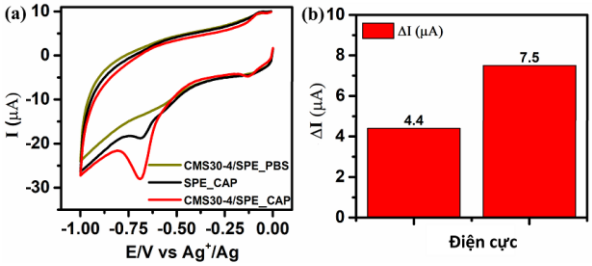

Figure 3.18 a) CV curves of CMS30-4/SPE electrode and SPE electrode in 0.1 M PBS solution (pH = 5.0) supplemented with 100µM CAP, the bar graph represents the CAP reduction peak current intensity signal.

In order to optimize the experimental conditions for analyzing CAP in pharmaceutical samples, we conducted research to investigate the effects of scanning speed and pH on the electrochemical performance of the CMS30-4/SPE electrode for CAP using the method CV scanning method. Results Figure 3.18 shows that scanning speed and pH have an impact on the ability to detect CAP using the CMS30-4/SPE electrode, and for pH = 5.0 and scanning speed of 60 mV/s the signal is detected, showing the highest CAP.

Figure 3.19 a shows the CV curve when the scanning speed (ν) changes from 10 to 60 mV/s, and two dependent plots (I_{pc} versus ν) and (E_{pc} versus lnν), with linear regression equation count:

$$\Delta I_{pc}\,(\mu A) = 0.102\ \nu\ (mVs^{-1}) + 1.204\ (R^2 = 0.99)$$

$$E_{pc} = -0.03\ \ln(\nu) - 0.788\ (R^2 = 0.99)$$

From the Laviron equation, the electron transfer coefficient (α) is determined to be 0.214, the number of electrons exchanged (n) is 4 and the electron transfer rate constant (k_s) is 1.75 s^{-1} . In addition, through the equation $I_{pc} = n^2F^2A\nu\Gamma/4RT$, where Γ is the adsorption capacity, A is the electrochemically active surface area and R, T and F have conventional meaning, it can be calculated. The amount of CAP adsorbed on the CMS30-4/SPE electrode surface is 3.488. 10^{-8} mol.cm^{-2}.

Figure 3.19 d shows the relationship between CAP reduction peak current intensity and pH when changing pH from 3 to 11, showing that at pH = 5.0 the peak current intensity value reaches the largest value, thus We choose pH value = 5.0 for the next experiments. Representing the dependence of the reduction peak position (E_{pc}) on pH, with the linear regression equation:

$$E_{pc} = -\ 0.04\ pH - 0.41\ (R^2 = 0.98)$$

We have the slope value of the standard curve - 0.040 V/pH, according to the Nernst equation (-0.059 m/n), with n and m being the number of electrons and protons participating in the reaction, respectively. The results showed that there were 4 electrons and 4 protons involved in the reaction of reducing the nitro group (R-NO_2) to the hydroxylamine group (R-NHOH), this result is consistent with the previously published reaction mechanism.

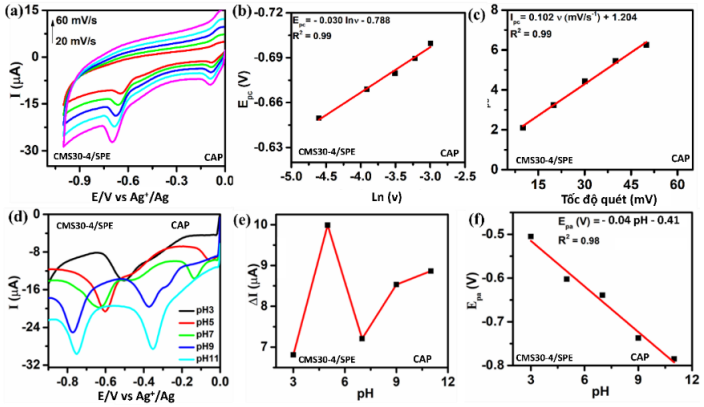

Figure 3.19. Results of investigating the influence of scanning speed (a, b, c); pH (d, e, f) for CAP detection of the CMS30-4/SPE electrode.

To evaluate the CAP detection performance of the electrochemical sensor based on CMS30-4/SPE, the DPV technique was performed to build a relationship between peak current and CAP antibiotic concentration in solution. The DPV curve and corresponding standard curve of the CMS30-4/SPE electrode in 0.1 M PBS buffer (pH = 5.0) with CAP concentrations varied from 1.0 µM to 50 µM are shown on Figure 3.20. Observing the DPV curves in a, we find that the CAP reduction peak current intensity at –0.6 V increases with CAP concentration in the range from 1.0 to 50 µM. The results of calculating and constructing a standard curve of the reduction peak current intensity according to CAP concentration are shown in Figure 3.20. The electrochemical sensor based on CMS30-4 material is linear in the CAP concentration range from 1.0 µM to 50 µM with the standard curve found as follows:

$$\Delta I_{pa} = 0.219\ C_{CAP}\,(\mu M) + 0.121,\ R^2 = 0.99$$

Electrochemical sensitivity of the measurement 2.0 μA μM^{-1} cm^{-2}, limit of detection (LOD) was 89 nM .

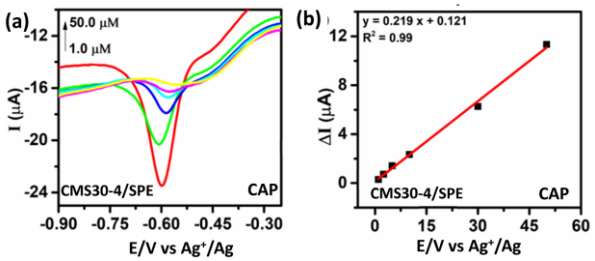

Figure 3.20. DPV curve represents electrochemical signal in 0.1M PBS solution (pH = 5.0) containing CAP with concentrations varying from 1.0 to 50 μM (a) and standard curve for determining CAP using an electrode CMS30-4/SPE (b).

Stability over time and repeatability is an important requirement for a sensor. To evaluate the above parameters of the sensor, we used the DPV method to determine the signal intensity of the CMS30-4/SPE electrode in 0.1M PBS solution (pH = 5.0) containing CAP. with a concentration of 100 μM. Figure 3.21a shows the results of stability survey in 3 times: day 1, day 7 and day 30 after manufacturing the CMS30-4/SPE sensor. The CAP reduction current signal retained 97 % of the original signal intensity after 30 days of storage at room temperature. The repeatability of the sensor is about 0.19% for 12 repeated measurements as shown in Figure 3.21. Reliability, high sensitivity, stability and good repeatability allow the application of the CMS30-4/SPE sensor in determining CAP content in pharmaceutical samples.

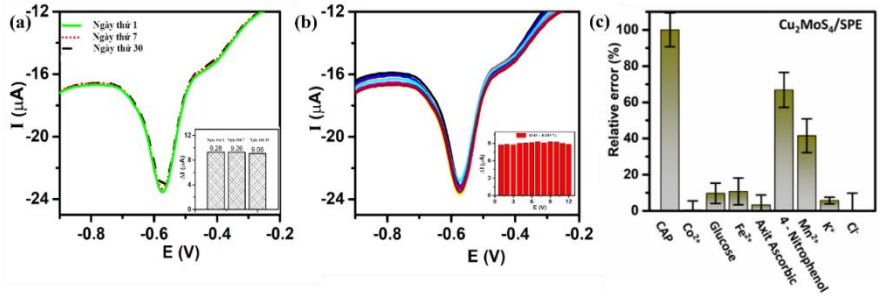

Figure 3.21: DPV curve investigating the stability (a), repeatability (b), and selectivity (c) of the CMS30-4/SPE electrode in 0.1M PBS solution (pH = 5.0) with contains CAP at a concentration of 100 μM.

Conclusion: The sensor electrode has been successfully fabricated CMS30-4/SPE by coating on SPE electrode base. The fabricated electrode has good stability and repeatability. The CAP concentration is linear in the concentration range from 1.0 to 50 μM according to the standard curve equation of the form y = 0.219 x + 0.121 with correlation coefficient R^2 = 0.99, LOD = 89 nM and electrochemical sensitivity 2.0 μA μM^{-1} cm^{-2} . The results of this research have been published in 01 domestic article belongs to the list of prestigious specialized magazines.

3.3.4. Electrochemical performance of CMS30-4/SPE towards P AR

CV technique was used to study the electrochemical activity of the CMS30-4/SPE sensor towards PAR. Measurements were performed in 0.1 M PBS solution (pH 7.4) containing 100 μM PAR, at a scan rate of 50 mV/s , results are shown in Figure 3.22. The PAR oxidation electrochemical signal was recorded on the CMS30-4/SPE electrode, with an I_{pa} value of 6.020 corresponding to an E_{pa} position of 0.310 V.

This result shows that the modification of the SPE electrode with CMS30-4 material has a significant effect on the electrochemical signal of the sensor system. At the same time, the peak intensity of the oxidation current has a signal nearly 2 times higher than the peak intensity of the PAR reduction current on SPE, so CMS30-4 has the potential to create a sensor to detect PAR by electrochemical method.

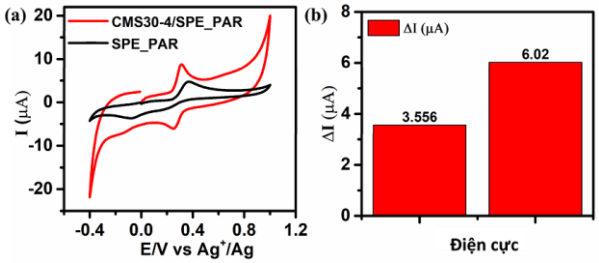

Figure 3.22. CV curve a) and signal bar graph b) of SPE and CMS30-4/SPE electrodes against PAR in PBS solution (pH = 7.4) containing 100 μM PAR.

The electrochemical kinetics of electron transfer of the PAR redox process is clarified when studying the influence of scanning speed on two parameters: maximum potential energy (E_{pa} and E_{pc}), and maximum current intensity (I_{pa} and I_{pc}). Figure 3.23a shows the CV curve of the modified electrode CMS30-4/SPE with scanning speed ν varying from 10 - 70 mV/s in 0.1 M PBS solution (pH = 7.4) containing PAR 100 μM, and two dependence plots (ΔI_{pc} ; ΔI_{pa} against $\nu^{1/2}$) and (E_{pc} ; E_{pa} against ln ν), with linear regression equation:

$$\Delta I_{pa}\,(\mu A) = 1.00\ \nu^{1/2}\,(mVs^{-1}) - 1.21 \qquad (R^2 = 0.99)$$

$$E_{pa} = 0.030 \ln(\nu) + 0.41 \qquad (R^2 = 0.99)$$

$$\Delta I_{pc}\,(\mu A) = 0.84\ \nu^{1/2}\,(mVs^{-1}) - 0.77 \qquad (R^2 = 0.99)$$

$$E_{pc} = 0.026 \ln(\nu) + 0.33 \qquad (R^2 = 0.99)$$

Figure 3.23 a and b, shows that the maximum current intensity increases linearly with increasing scanning speed, this result confirms that the PAR redox reaction occurring at CMS30-4/SPE is a process controlled by the diffusive.

From the graph showing the dependence of ΔI_{pc} ; ΔI_{pa} according to ν, calculate the adsorption degree (r) according to equation (**):

$$\Delta I_{pa}\,(\mu A) = 0.087\ \nu\,(mVs^{-1}) - 1.21 \qquad (R^2 = 0.99)$$

$$\Delta I_{pc}\,(\mu A) = 0.046\ \nu^{1/2}\,(mVs^{-1}) - 0.77 \qquad (R^2 = 0.98)$$

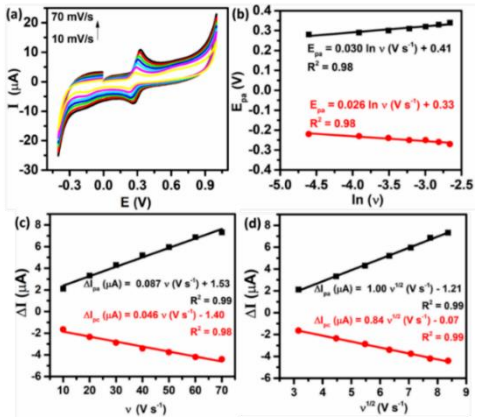

Figure 3.23. Investigate the effect of scanning speed on the PAR detection signal of an electrochemical sensor based on CMS30-4 material.

We have r_{pa} = 1.146. 10^{-7} moles. cm^{-2} and r_{pc} = 6.059. 10^{-8} mol. $cm^{-2,}$ it can be seen that the adsorption capacity of the oxidation direction is 1.89 times higher than the reduction direction. Therefore, we chose the PAR oxidation process to conduct further investigation experiments.

The electrochemical oxidation mechanism of PAR occurring on the CMS30-4/SPE electrode was studied using the DPV technique, through the influence of pH on the electrochemical performance of PAR detection. Figure 3.24 presents the effect of pH on the PAR detection signal for oxidation (Figure 3.24).

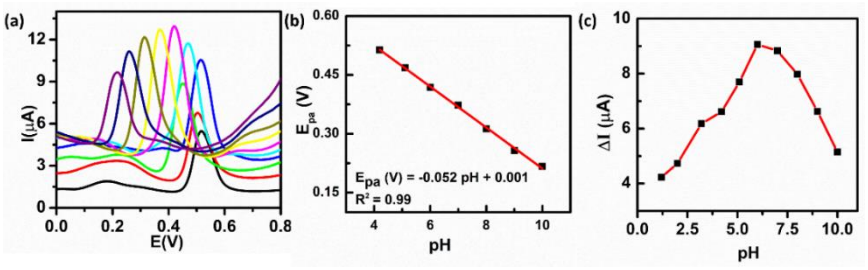

Figure 3.24. Investigate the effect of pH on the PAR detection signal of an electrochemical sensor based on CMS30-4 material.

Figure 3.24a, shows that the maximum oxidation potential of PAR shifts towards the negative side as the pH value increases, demonstrating the participation of protons in the electrochemical oxidation process of PAR. From the DPV curve (Figure 3.24 b) when the pH of the buffer solution changes from 1 to 10, a dependence chart (E_{pa} versus pH) can be drawn, with a linear regression equation:

$$E_{pa} = - 0.052\ pH + 0.001\ (R^2 = 0.99)$$

We have the slope value of the standard curve - 0.052 V/pH, according to the Nernst equation (-0.059 m/n) V/pH, with n and m being the number of electrons and protons participating in the reaction, respectively. The results show that the ratio m/n is equal to 1, combined with the equation E_{pa} = 0.030 ln (v) + 0.41 to determine m = n = 2 and α = 0.572. The obtained results correspond to other published results studying redox reactions in PAR. At the same time, the oxidation peak current of PAR gradually increases from pH 1.3 to 6.0 and gradually decreases when the pH value is greater than 6.0. Therefore, pH 6.0 was chosen in subsequent electrochemical experiments.

The electrochemical sensor based on the modified electrode CMS30-4/SPE was used to determine PAR content using DPV technique, under pH = 6.0 conditions. The DPV curves in Figure 3.25 a, show that the PAR oxidation peak current increases as the concentration varies between 0.156 and 100 μM. The resulting calibration plots demonstrate a good linear relationship between the Oxidation peak current and PAR concentration in the concentration range from 0.156 to 90 μM, with the regression equation:

$$\Delta I_{pa}\ (\mu A) = 0.147\ C_{PAR}\ (\mu M\ ) + 0.279\ (R^2 = 0.99)$$

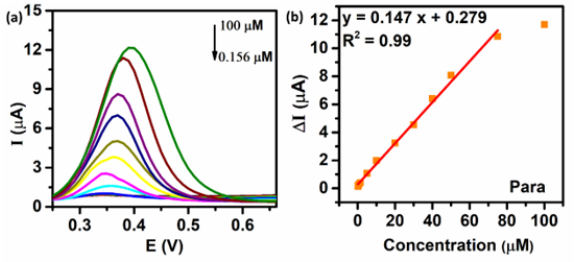

Figure 3.25. a) DPV curve and b) standard curve representing the electrochemical signal of CMS30-4/SPE electrode in 0.1 M PBS solution (pH = 6.0) containing PAR with concentrations varying from 0.156 to 100 µM.

The limit of detection (LOD) of the electrochemical sensor was determined to be 45 nM, the electrochemical sensitivity of the material was calculated to be 1.336 µA μM^{-1} cm^{-2}. The analytical parameters of the electrochemical sensor based on CMS30-4 for PAR detection were compared with several sensors reported in recent publications. These results indicate that the proposed CMS30-4-based material has good performance for PAR detection electrochemical oxidation with high electrochemical sensitivity, relatively low detection limit, and linear range. broadness.

3.3.5. Sensor stability and repeatability

The stability of the sensor was studied through DPV signals at 3 times: day 1, day 14 and day 60 after manufacturing the CMS30-4/SPE sensor. The PAR oxidative current signal retained 99.28 % and 99.22 % of the original signal intensity after 14 and 60 days of storage at room temperature Figure 3.26 a and b). The repeatability of the proposed electrochemical sensor was evaluated by conducting 20 consecutive DPV measurements in a 0.1 M PBS solution (pH = 6.0) containing 100 µM, the results are presented in Figure 3.26 c, shows that the electrochemical signal of the PAR detection oxidation reaction does not change significantly after 15 measurements, with standard deviation value SD = 0.015.

The selectivity of the sensor was studied by adding a 10-fold concentration of potential interfering substances (K^+, Na^+), antibiotics (cripproxacin, roxithromycin, ibuprofen, azithromycin, erythromycin) in the PAR solution 20 µM. The results of Figure 3.26d indicate that these substances did not cause significant changes to the electrochemical signal of PAR detection, except for azithromycin.

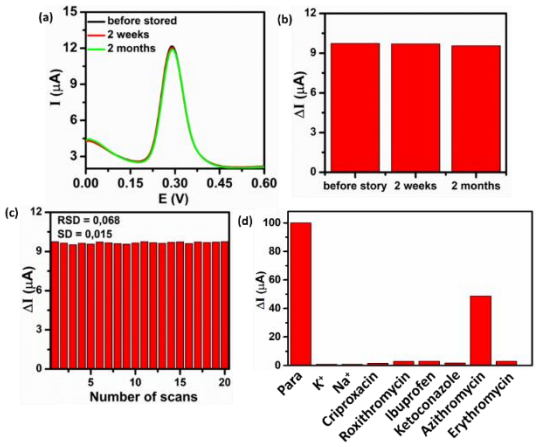

Figure 3.26. Stability (a, b), repeatability (c), and selectivity (d) of the electrochemical sensor of the CMS30-4/SPE electrode in 0.1 M PBS solution (pH = 6.0) containing 100 μM PAR.

Conclusion: The process for determining CAP using the electrochemical sensor method based on CMS30-4 material has good repeatability and selectivity, but care should be taken to separate azithromycin from samples containing PAR before analysis.

3.4. COMPARISON OF ELECTROCHEMICAL PERFORMANCE OF SENSORS BASED ON MOLYBDENDEN SUNFIDE AND COPPER MOLYBDEN SUNFIDE MATERIALS

The parameters of electrochemical sensors based on NP-MoS_2 and Cu_2MoS_4 (CMS30-4) materials to detect OFX, PAR and CAP are summarized in Table 3.3.

Table 3.3. Comparison table of electrochemical parameters of MoS_2 and Cu_2MoS_4 electrodes for detection of OFX, CAP and PAR

Material specifications				**Sensor parameters**					
Electrode	**A (cm^2)**	**R_{ct} (Ω)**	**k^0 ($cm\,s^{-1}$)**	**E (V)**	**I (µA)**	**Linear range (µM)**	**LOD (µM)**	**Sensitivity**	**Repeatability (RSD%)**
				OFX detection sensor					
CMS30-4/SPE	0.202	164.5	$1,60 \times 10^{-6}$	0.710	9.629	0.625- 100	0.067	1.17	0.540
				PAR detection sensor					
				-0.71	7.5	0.156-100	0.045	1.34	0.190
				CAP detection sensor					
				0.310	6.020	1.0-50	0.089	2.0	0.185
NP-MoS_2 /SPE	0.253	341.2	0.76×10^{-6}	**OFX detection sensor**					
				0.738	4.583	5.0-75	2.5	0.518	0.242
				PAR detection sensor					
				0.362	4.131	5.0- 100	0.76	0.28	0.108
				CAP detection sensor					
				-0.66	6.02	10-70	5.0	1.22	0.839

Conclusion: The surface active area (A) values of the NP-MoS_2 /SPE electrode are 1.25 times larger than those of CMS30-4/SPE, however the charge transfer resistance (R_{ct}) of CMS30-4/SPE is nearly half the resistance value of the NP-MoS_2/SPE electrode. This result shows that the factor that enhances electrical conductivity and electrocatalytic activity is the main reason for increasing the electron transfer rate on the CMS30-4/SPE electrode surface. This leads to the electrochemical sensor based on CMS30-4 material having higher sensitivity, limit, repeatability, and lower LOD than the sensor based on NP-MoS_2 material for molecular substances OFX, CAP and PAR.

3.5. APPLICATION OF ANALYSIS OF OFX, CAP AND PAR IN PHARMACEUTICALS

The content of OFX, CAP and PAR in commercial pharmaceutical samples was determined according to the procedure in Figure 3.27.

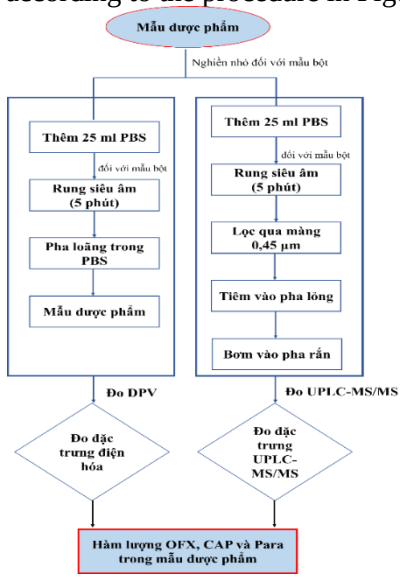

Figure 3.27. Procedure for determining OFX, PAR, CAP in pharmaceuticals.

CMS30-4 material was selected to manufacture 3 CMS30-4/SPE electrodes with the same manufacturing process. The results of the analysis are presented in Table 3.4, each result is the average value of 3 repeated measurements.

Table 3.4. Results of OFX, PAR and CAP content in pharmaceuticals

	Electrochemical sensing method (mg)	**Method UPLC-MS/MS (mg)**	**Error between two measurements (%)**
Ofloxacin 200 mg			
Electrode 1	207.300	204.216	1.51
Electrode 2	208.000	204.12 0	1.90
Electrode 3	202.800	204.789	0.97
TB	206.033	204.042	1.46
Chloramphenicol 200mg			
Electrode 1	263.764	256.194	2.87
Electrode 2	254.815	245.998	3.46
Electrode 3	260.435	253.143	2.80
TB	259.671	251.439	3.04
Paracetamol 500 mg			
Electrode 1	469.880	458.980	2.40
Electrode 2	468.840	447.950	2 .05
Electrode 3	474.54 0	448.97 0	2.79
TB	471.086	451.967	2.41

From Table 3.4, obtain the results of analysis of OFX, CAP and PAR content in pharmaceuticals using the CMS30-4/SPE electrochemical sensor as follows:

- OFX content in the tablet sample is 206.033 (mg/tablet), an average difference of 1.46 % compared to the method. UPLC-MS/MS.

- The CAP content in the tablet sample is 259.61 (mg/tablet), an average difference of 3.04 % compared to the method. UPLC-MS/MS.

- The PAR content in the tablet sample is 471.086 (mg/tablet), an average difference of 2.41 % compared to the method. UPLC-MS/MS.

Conclusion: The sensor has also been used in practical applications to analyze the content of the above substances in pharmaceutical samples, the error with UPLC-MS/MS measurement is < 5 %. The developed analytical procedure can be applied to field sample analysis.

CONCLUSIONS AND RECOMMENDATIONS

1. Successfully fabricated crystalline MoS_2 nanoparticles with large specific surface area. Electrochemical sensors based on this material determine CAP, PAR and OFX with limited, repeatable and low sensitivity.

2. Successfully synthesized Cu_2MoS_4 nanomaterials by hydrothermal method, with 3 morphologies: solid bar (CMS10-3), hollow bar (CMS30-3) and plate (CMS30-4). CMS materials all have large specific surface areas, improving electrical conductivity and ion exchange compared to MoS_2 materials.

3. The study also demonstrated the outstanding electrocatalytic activity of Cu_2MoS_4 nanomaterials in sheet form.

The sensor determines Ofloxacin with a concentration range of 0.625 to 100 μM, calibration curve y = 0.129 x - 0.068 with R^2 = 0.99, limit of detection (LOD) of 67 nM, electrochemical sensitivity achieved is 1.17 μA μM^{-1} cm^{-2}. Analysis of OFX content in tablet samples using Cu_2MoS_4/SPE electrochemical sensor is 206.033 (mg/tablet), an average difference of 1.461% compared to the method UPLC-MS/MS.

Standard curve for determining Paracetamol using CMS30-4/SPE sensor electrode in linear range: from 0.156 - 90 μM (R^2 = 0.99), electrochemical sensitivity 1.336 μA μM^{-1} cm^{-2}, LOD = 45 nM. Electrochemical sensors with good selectivity and repeatability have been applied to determine PAR content in tablet samples whose main ingredient is PAR with < 3% difference compared to the packaging.

The standard curve for determining Chloramphenicol is linear in the concentration range from 1.0 to 100 μM according to the standard curve

equation of the form y = 0.219 x + 0.121, R^2 = 0.99 and sensitivity 2.0 µA μM^{-1} cm^{-2}, LOD = 89 nM. The sensor is selective with organic substances (glucose, ascorbic acid) and ions (K^+, Co^{2+}, Fe^{2+}, Cl^-), whereas Mn^{2+} and 4-nitrophenol have an effect on CAP detection signal strength. Analyzing real samples, the error results compared to the CAP content were listed on the label range from 1.93 - 5.51%.